American Mineralogist, Volume 95, pages 1758–1764, 2010

Compressibility of protoamphibole: A high-pressure single-crystal diffraction study of protomangano-ferro-anthophyllite

P.F. Zanazzi,[1,*] F. Nestola,[2] and D. Pasqual[2]

[1]Dipartimento di Scienze della Terra, Università di Perugia, Piazza Università, I-06123 Perugia, Italy
[2]Dipartimento di Geoscienze, Università di Padova, Via Giotto 1, I-35137 Padova, Italy

Abstract

The high-pressure behavior of protoamphibole (space group *Pnmn*) was studied by in situ single-crystal X-ray diffraction on a sample of protomangano-ferro-anthophyllite with formula $(Mn_{1.39}Fe_{0.59})(Fe_{3.98}Mg_{1.02})Si_8O_{22}(OH)_2$, from Yokone-Yama, Awano Town, Tochigi Prefecture, Japan. Unit-cell parameters were collected at various pressures up to 9 GPa, and structural refinements were obtained from data collected at several pressures up to 7 GPa. Fitting the *P*-*V* data to a third-order Birch-Murnaghan equation of state (EoS) gives the following parameters: K_{T0} = 64(1) GPa, K' = 7.0(4), and V_0 = 926.4(4) Å^3. Axial moduli are: K_{0a} = 30.7(8) GPa, K'_a = 10.8(5), and a_0 = 9.430(2) Å; K_{0b} = 109(4) GPa, K'_b = 2.7(8), and b_0 = 18.364(4) Å; K_{0c} = 94(5), GPa, K'_c = 4(1), and c_0 = 5.354(2) Å. The corresponding axial compressibilities (10^{-3} GPa^{-1}) are β_a = 10.9(3), β_b = 3.1(1), and β_c = 3.5(2), and indicate that the HP behavior of protomangano-ferro-anthophyllite is highly anisotropic, the highest compressibility being along [100]. No discontinuous behavior or polymorphic transitions were observed in the pressure range studied.

Structural refinements show that M1, M2, and M3 polyhedra have similar compressibilities, owing to their similar composition. M4 (72% Mn, 28% Fe) is a highly distorted site and is slightly softer than the other octahedra. The major movements in the tetrahedral ribbon concern kinking of the double chain, bending along the [100] direction through the empty A site, and tetrahedral rotation, necessary to maintain coherence with the octahedral layer. The kinking angle of O5-O6-O5, which in air is 179.1(2)°, decreases to 174(2)° at 6.9 GPa. The T1-O7-T1 angle changes from 143.8(3)° to 134(5)° at 6.9 GPa, and the tetrahedral rotation α increases from 0.2(2)° to 4(2)°.

Keywords: Protoamphibole, protomangano-ferro-anthophyllite, compressibility, equation of state, high-pressure structure

Introduction

Amphiboles are important rock-forming minerals that have been extensively studied from the crystallographic, mineralogical, and petrologic points of view. Their structural and chemical features are summarized in several reviews (e.g., Hawthorne 1981; Hawthorne et al. 2007). Amphiboles are chain silicates, with a double tetrahedral chain extending along the **c** axis. Their basic structural units are represented by tetrahedral-octahedral-tetrahedral layers (T-O-T) parallel to (100), the so-called *I*-beams (Thompson 1970). Adjacent T-O-T layers are staggered ±**c**/3 with respect to one another, generating several amphiboles polymorphs with different space groups: *C*2/*m*, *P*2$_1$/*m*, *P*2/*a*, *Pnma*, *Pnmn*, *C*$\bar{1}$. The more widespread amphiboles are monoclinic, with the *I*-beam stacking sequence along [100] ...+ +... or ...– –..., and space group *C*2/*m* (structure type tremolite) or *P*2$_1$/*m* (cummingtonite). Another group comprises the orthorhombic amphiboles, with space group *Pnma* and sequence ...+ + – –... (anthophyllite). A less widespread structure type of orthorhombic amphiboles is that of protoamphibole, with stacking sequence ...+ – + –... and space group *Pnmn*. The first protoamphibole to be studied was a synthetic phase containing Mg, Li, and F (Gibbs et al. 1960). Some natural phases having this structure type were found later (Matsuura and Sueno 1984: Matsuura et al. 1985). Owing to their composition, these amphiboles were called protoferro-anthophyllite (PFA) and protomangano-ferro-anthophyllite (PMFA). PFA came from fayalitic masses of granitic pegmatite of Cheyenne Canyon and Cheyenne Mountain, U.S.A.; PMFA from manganese ore deposits at Suisho-Yama and granitic pegmatite at Yokone-Yama, Japan. Neither PFA and PMFA contain Li or F, but they have a chemical composition similar to that of the monoclinic polymorph grunerite. Their structure was first described by Sueno et al. (2002). The structure of protoamphibole projected along [001] is reported in Figure 1. The key differences between *Pnmn* (protoamphibole) and *Pnma* (anthophyllite) structures are (1) the two double-chains of tetrahedra in the *I*-beam unit are equivalent in *Pnmn*, but are non-equivalent in *Pnma*; and (2) the point symmetry of M4 site is 2 on the diad in *Pnmn*, and 1 in *Pnma*. Both these differences can be significant particularly in relation to their HP/HT behavior, owing to the extra freedom to deform for anthophyllite that is not available to protoamphibole.

Since amphiboles are the most widespread hydrous minerals in the lithospheric mantle, playing a key role in governing the petrologic and geochemical development of metasomatic processes (Vannucci et al. 1995; Ionov and Hofmann 1995; Ionov

* E-mail: zanazzi@unipg.it

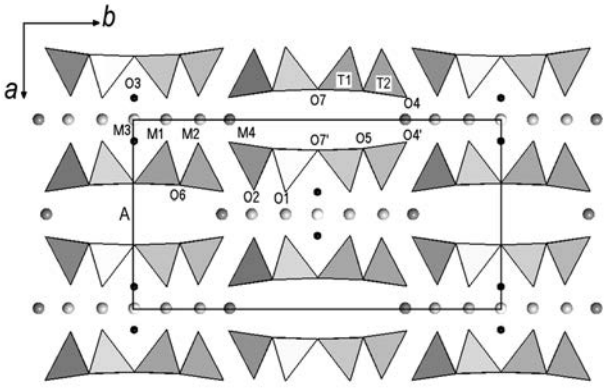

FIGURE 1. Structure of protomangano-ferro-anthophyllite projected along [001].

et al. 2002; Wallace and Green 1991; Niida and Green 1999), assessment of their thermochemical and thermophysical properties is important for calculation of phase equilibria.

Despite the large amount of data published on amphiboles, very few studies on their structural behavior in non-ambient conditions have been carried out (Welch et al. 2007). In particular, the effect of pressure on their structural behavior is not yet well constrained, as measurements of compressibility and structural changes with pressure are scarce. In situ single-crystal X-ray diffraction studies have been reported for tremolite, pargasite, and glaucophane up to 4 GPa (Comodi et al. 1991) and for grunerite up to 5.1 GPa (Zhang et al. 1992). The compressibility of synthetic K-richterite [Welch and Lennie, unpublished results reported in Welch et al. (2007)] has been determined by synchrotron powder data using Rietveld refinement. The compressibility of two polymorphs on the cummingtonite-grunerite join up to 8 GPa, and the effect of pressure on the *C2/m-P*2_1*/m* phase transition of cummingtonite have been reported (Yang et al. 1998; Boffa Ballaran et al. 2000). The HP behavior of kaersutite has been recently described (Comodi et al. 2010). Until now, no in situ HP studies of orthorhombic amphiboles have been made. To improve knowledge of the HP behavior of orthoamphibole, the effect of pressure on the structure of *Pnmn* protoamphibole was studied by single-crystal X-ray diffraction, using a diamond anvil cell (DAC) in the range 10^{-4}–9 GPa.

EXPERIMENTAL METHODS

Several colorless transparent bladed crystals of a natural protomangano-ferro-anthophyllite (PMFA) sample from Yokone-Yama, Awano Town, Tochigi Prefecture, Japan, kindly supplied by Masa Kurosawa (Institute of Geoscience, University of Tsukuba), were selected for high-pressure X-ray diffraction experiments. Their chemical composition was determined at the "Istituto di Geoscienze e Georisorse," CNR Padova (Italy) on a CAMECA-CAMEBAX electron microprobe operating with a fine-focused beam (~1 μm) at an accelerating voltage of 15 kV and a beam current of 15 nA in wavelength dispersive mode (WDS), with 10 s counting times for peak and 5 s for total background. X-ray counts were converted into oxide wt% using the PAP correction program (Pouchou and Pichoir 1985). The oxide percent by weight obtained by averaging 16 microprobe spots gave the following formula: $(Mn_{1.39}Fe_{0.59})(Fe_{3.98}Mg_{1.02})Si_8O_{22}(OH)_2$, very similar to the composition of the sample described by Sueno et al. (2002). The amphibole composition and analysis conditions used are listed in Table 1.

High-pressure lattice measurements

Unit-cell parameters were measured at various pressures up to 9 GPa by single-crystal X-ray diffraction at the Dipartimento di Geoscienze, University of Padova. A sample of PMFA with dimensions 0.10 × 0.06 × 0.04 mm was loaded with a fragment of α quartz in an ETH diamond anvil cell (DAC) (Miletich et al. 1999), equipped with type-I diamonds having a 600 μm diameter culet face. The pressure chamber was a 250 μm diameter hole, drilled in a 250 μm thick steel Inconel 750X gasket preindented to 150 μm. A methanol-ethanol mixture (4:1 by volume) was used as hydrostatic pressure-transmitting medium. The quartz crystal was used for precise measurement of pressure (Angel et al. 1997). Uncertainties in pressure calibration are based on the EoS of quartz and are between ±0.2 and ±0.8 GPa. Experiments were carried out at 10^{-4}–9 GPa. Unit-cell parameters were determined at each pressure by centering 12–15 Bragg reflections between 15° and 30° in 2θ with a four-circle Huber diffractometer operating at 50 kV and 40 mA (Mo*K*α). During the centering procedure, the effects of crystal offsets and diffractometer aberrations were eliminated from refined peak positions by the eight-position centering method of King and Finger (1979). Unit-cell parameters at various pressures are given in Table 2.

Room-pressure data collection

For refinement at room conditions, numerous crystals were mounted at the Dipartimento di Scienze della Terra, University of Perugia, on an XCALIBUR (Oxford Diffraction) diffractometer equipped with CCD area detector, operating at 50 kV and 35 mA, with graphite monochromated Mo radiation (λ $K\alpha_1$ = 0.7093 Å). All samples displayed diffuse streaks along **a***. This feature, already found by Gibbs (1969) and Sueno et al. (1998, 2002), was ascribed to stacking faults resulting in polysynthetic twinning crystals or to intergrowths of oriented clino- and orthoamphibole lamellae. After rejection of several samples, one crystal fragment (of about 0.15 × 0.08 × 0.05 mm) showing less streaking was chosen

TABLE 1. Representative analysis (wt%) and structural formula of protomangano-ferro-amphibole

Oxides	(wt%)	Spectrum line, analyzer crystal, and standard	Elements	Cation distribution
SiO_2	48.9(2)	*K*α, TAP,diopside	Si	7.956
FeO	33.6(3)	*K*α, LIF, Fe_2O_3	Al	0.034
MnO	10.1(1)	*K*α, LIF, $MnTiO_3$	Total T	8.000
MgO	4.2(1)	*K*α, TAP, MgO	Fe^{2+}	3.874
CaO	0.25(2)	*K*α, PET, diopside	Mg	1.018
Al_2O_3	0.18(2)	*K*α, TAP, Al_2O_3	Fe^{3+}	0.103
Na_2O	0.05(5)	*K*α, TAP, albite	Cr	0.003
TiO_2	0.02(2)	*K*α, LIF, $MnTiO_3$	Ti	0.002
Cr_2O_3	0.02(2)	*K*α, LIF, Cr_2O_3	Total M1,2,3	5.000
K_2O	0.01(1)	*K*α, PET, orthoclase	Mn^{2+}	1.388
Cl	0.05(2)	*K*α, PET, vanadinite	Fe^{2+}	0.594
			Total M4	1.98
Total	97.38		Cl	0.01
			OH	1.99
			Total X	2.000

Note: The content of 0.044 Ca, 0.002 K, and 0.016 Na apfu resulting from the analysis were ascribed to intergrowths of oriented clino- and orthoamphibole lamellae. Fe^{3+} was calculated on the basis of charge balance.

TABLE 2. Lattice parameters of protomangano-ferro-anthophyllite as a function of *P*

P (GPa)	*a* (Å)	*b* (Å)	*c* (Å)	*V* (Å³)
0.0001	9.4276(9)	18.356(3)	5.3503(6)	925.9(2)
0.504(7)*	9.3843(9)	18.335(3)	5.3434(6)	919.4(2)
1.340(8)	9.3206(9)	18.290(3)	5.3300(6)	908.6(2)
1.796(7)	9.2895(7)	18.271(3)	5.3237(5)	903.6(2)
2.563(6)	9.2406(8)	18.230(3)	5.3114(5)	894.7(2)
3.291(9)*	9.2017(9)	18.193(3)	5.2978(6)	886.9(2)
3.930(9)	9.1681(7)	18.157(3)	5.2853(6)	879.8(2)
4.702(10)*	9.1350(6)	18.117(2)	5.2725(4)	872.6(1)
5.474(8)	9.1043(5)	18.073(2)	5.2597(3)	865.4(1)
5.899(12)*	9.0865(4)	18.054(2)	5.2529(3)	861.7(1)
7.297(12)	9.0378(4)	17.985(2)	5.2320(3)	850.45(9)
8.116(13)*	9.0134(4)	17.950(1)	5.2209(3)	844.70(9)
8.964(12)	8.9891(3)	17.916(1)	5.2105(3)	839.16(8)

* Measured in decompression.

for the HP structural study.

Diffraction data were first collected from the sample in air. To maximize reciprocal space coverage, a combination of ω and φ scans was used, with a step size of 0.8° and a time-frame of 50 s, for a total of 3500 frames. The distance crystal-area detector was 65 mm, 2θ range 5–67°. Data were corrected for absorption with the SADABS program (Sheldrick 1996). Details of data collection and refinement are listed in Table 3.

Crystal structure refinement was carried out in space group *Pnmn* with anisotropic displacement parameters using SHELX-97 program (Sheldrick 1997), starting from the atom coordinates of Sueno et al. (1998). Neutral atomic scattering factors and $\Delta f'$, $\Delta f''$ coefficients from *The International Tables for Crystallography* (Wilson and Prince 1999) were used. Full occupancy was assumed for all cation sites. The electron density at these sites was accounted for by fitting the scattering factor curves of Fe and Mg for sites M1, M2, and M3, and Mn and Fe for site M4, with variable occupancy. At the end of the refinement, the contribution of the H atom linked to O3 was included and refined, constraining the O-H distance to 0.9 ± 0.02 Å, and a thermal parameter fixed at 0.05 Å^2. The resulting sum of electrons for the cations in octahedral sites in the cell was 330.6 e$^-$. Taking into account the quality of the crystals and of the diffraction data, this value is in good agreement with data calculated for two formula units on the basis of chemical analysis (331.7 e$^-$; Table 1). Table 4[1] lists observed and calculated structure factors. Atomic coordinates and displacement parameters are listed in Table 5.

High-pressure data collection

For the HP structural study, the same PMFA crystal as studied at room conditions was loaded in the same ETH DAC used for the HP lattice parameter measurements. The pressure chamber was a 300 µm diameter hole, drilled in a 250 µm thick steel Inconel 750X gasket pre-indented to 180 µm. A methanol:ethanol mixture (4:1) was used as a hydrostatic pressure-transmitting medium. Experiments were carried out in the pressure range 10^{-4}–6.9 GPa. The DAC was centered on the diffractometer following the procedure of Budzianowski and Katrusiak (2004). Intensity data were collected with a CCD detector. To maximize reciprocal space coverage, a combination of ω and φ scans was used, with a step size of 0.8° and a time-frame of 50 s; the 2θ range was 5–57° ; the unit-cell parameters were measured from the angles of the whole set of collected data. Pressure calibration was based on the EoS of the protoamphibole previously determined, starting from the value of the unit-cell volume determined at each pressure. Data were measured at 0.0001 GPa (in DAC without liquid) and at 1.54, 2.23, 3.92, 6.02, and 6.93 GPa. The uncertainty in P is estimated to be of the order of 0.1 GPa. To improve the observation/parameter ratio, determination of structural parameters at 2.23 and 3.92 GPa was carried out by merging the reflections from two different mountings of the sample reoriented in DAC at nearly the same pressure, after due corrections.

Intensity data were corrected for cell and crystal absorption with Absorb V6.1 software (Angel 2004a). Least-squares refinements were performed with the SHELX-97 program (Sheldrick 1997). To reduce the number of refined parameters, structural refinements with the crystal in DAC were carried out with isotropic displacement factors (IDF) constraining all the T-, M-, and O- to share one IDF value per group (Table 5). Site occupancies were fixed at those resulting from the refinement in air. Details of data collections and refinement are listed in Table 3. Observed and calculated structural factors are shown in Table 4[1]. Fractional atomic coordinates and displacement parameters are listed in Table 5.

[1] Deposit item AM-10-058, Table 4 and CIFs. Deposit items are available two ways: For a paper copy contact the Business Office of the Mineralogical Society of America (see inside front cover of recent issue) for price information. For an electronic copy visit the MSA web site at http://www.minsocam.org, go to the *American Mineralogist* Contents, find the table of contents for the specific volume/issue wanted, and then click on the deposit link there.

Results

Equation of state and compressibility

The changes of the unit-cell parameters and volumes of PMFA with pressure are shown in Table 2 and Figure 2. They show a steady change with pressure. No evidence for discontinuous behavior or phase transitions was found in the investigated pressure range; all the cell parameters decrease monotonically.

A plot of the normalized stress F_E vs. Eulerian finite strain f_E (Jeanloz and Hazen 1991; Angel 2000) indicates that $K' > 4$ (Fig. 3). Therefore, a third-order Birch-Murnaghan EoS (BM3-EoS) was used to fit the pressure-volume (P-V) data by simultaneously refining unit-cell volume at room pressure V_0, bulk modulus K_{T0} and its first pressure derivative K' with the EOS-FIT V6.1 program (Angel 2004b). Weights were used that were based upon the e.s.d. values on P and V. The refined EoS parameters are: K_{T0} = 64(1) GPa, K' = 7.0(4), and V_0 = 926.4(4) Å^3. These values match those obtained from weighted linear fits through F-f data: K_{T0} = 65.7(9) GPa, K' = 6.5(6).

The axial moduli of PMFA were calculated by means of a parameterized form of the BM3-EoS, in which a, b, and c parameters are cubed and fitted as volumes with the EOS-FIT V6.1 program (Angel 2004b). The resulting EoS parameters are: K_{0a} = 30.7(8) GPa, K'_a = 10.8(5), and a_0 = 9.430(2) Å; K_{0b} = 109(4) GPa, K'_b = 2.7(8), and b_0 = 18.364(4) Å; K_{0c} = 94(5) GPa, K'_c = 4(1), and c_0 = 5.354(2) Å. Axial compressibilities, obtained from the relation $\beta = 1/3(K_0^{-1})$ and expressed in 10^{-3} GPa^{-1}, are: β_a = 10.9(3), β_b = 3.1(1), β_c = 3.5(2). These values show that the HP behavior of protomangano-ferro-anthophyllite is highly anisotropic, the highest compressibility being along [100]. These values may be compared with those of linear compressibilities—6.8(2), 2.4(3), and 2.8(1)—measured along [100], **b** and **c**, respectively, for $C2/m$ cummingtonite (Yang et al. 1998) and with the respective values of 4.97(6), 3.50(4), and 3.62(5) of grunerite (Zhang et al. 1992).

Structural evolution with *P*

Bond distances, polyhedral volumes, and relevant geometrical parameters in air and at various pressures are listed in Table 6. The ambient structure determined here is in excellent agreement with that reported by Sueno et al. (1998). Since the details of protoamphibole structure have been thoroughly discussed by Gibbs (1969), they will not be repeated here. The inevitably lower quality of HP data sets, due to the far fewer unique intensities collected as a result of the limited access to reciprocal space imposed by the DAC, precluded a detailed analysis of polyhedral volumes. However, it is clear that the empty A site is the softest component of the structure and is correlated with the behavior

Table 3. Details of data collection and refinement of protomangano-ferro-anthophyllite at various pressures

P (GPa)	0.0001	0.0001*	1.54	2.23	3.92	6.02	6.93
a (Å)	9.444(1)	9.450(4)	9.320(4)	9.279(4)	9.186(5)	9.101(6)	9.076(6)
b (Å)	18.364(3)	18.368(7)	18.266(7)	18.226(7)	18.140(5)	17.990(4)	17.944(5)
c (Å)	5.3575(7)	5.354(2)	5.322(2)	5.310(2)	5.283(2)	5.259(2)	5.242(2)
V (Å^3)	929.2(6)	929.3(9)	906(1)	898(1)	880(1)	861(1)	854(1)
No. measured reflections	8892	2181	2586	5296	4947	3906	3349
No. indep. reflections	1807	235	276	317	328	377	310
Reflections with $I > 2\sigma(I)$	1302	163	184	201	192	159	183
No. refined parameters	106	33	33	34	34	33	33
R_{int}%	2.75	6.7	8.4	9.7	10.0	11.6	12.4
R_1%	4.22	6.1	5.9	6.7	6.4	7.3	9.3

*Data collected with the sample in DAC.

TABLE 5. Atom coordinates and isotropic equivalent displacement parameters (Å²) of protomangano-ferro-anthophyllite at various pressures

P (GPa)	0.0001	0.0001*	1.54	2.23	3.92	6.02	6.93
				T1			
x	0.2844(1)	0.283(2)	0.289(1)	0.289(1)	0.290(1)	0.287(4)	0.287(3)
y	0.08379(5)	0.0836(3)	0.0837(3)	0.0837(2)	0.0841(3)	0.0840(5)	0.0842(4)
z	0.1640(2)	0.167(1)	0.159(1)	0.159(1)	0.158(1)	0.149(3)	0.152(2)
U_{iso}/U_{eq}	0.0066(2)	0.008(1)	0.008(1)	0.008(1)	0.008(1)	0.007(2)	0.007(2)
				T2			
x	0.2958(1)	0.295(1)	0.298(1)	0.300(1)	0.300(1)	0.298(3)	0.294(3)
y	0.16763(5)	0.1678(3)	0.1677(3)	0.1679(3)	0.1677(3)	0.1679(5)	0.1682(4)
z	0.6610(2)	0.661(1)	0.654(1)	0.655(1)	0.651(1)	0.652(3)	0.654(2)
U_{iso}/U_{eq}	0.0072(2)	0.008(1)	0.008(1)	0.008(1)	0.008(1)	0.007(2)	0.007(2)
				M1†			
x	0	0	0	0	0	0	0
y	0.08797(4)	0.0881(2)	0.0872(2)	0.0870(2)	0.0861(2)	0.0853(4)	0.0853(4)
z	½	½	½	½	½	½	½
U_{iso}/U_{eq}	0.0082(2)	0.010(1)	0.0116(9)	0.0097(8)	0.0103(9)	0.012(2)	0.010(1)
				M2†			
x	0	0	0	0	0	0	0
y	0.17963(4)	0.1796(3)	0.1780(2)	0.1781(2)	0.1773(2)	0.1778(5)	0.1771(4)
z	0	0	0	0	0	0	0
U_{iso}/U_{eq}	0.0080(2)	0.010(1)	0.0116(9)	0.0097(8	0.0103(9)	0.012(2)	0.010(1)
				M3†			
x	0	0	0	0	0	0	0
y	0	0	0	0	0	0	0
z	0	0	0	0	0	0	0
U_{iso}/U_{eq}	0.0074(3)	0.010(1)	0.0116(9)	0.0097(8	0.0103(9)	0.012(2)	0.010(1)
				M4†			
x	0	0	0	0	0	0	0
y	0.26056(4)	0.2605(2)	0.2606(2)	0.2604(2)	0.2604(2)	0.2608(4)	0.2608(3)
z	½	½	½	½	½	½	½
U_{iso}/U_{eq}	0.0116(2)	0.010(1)	0.0116(9)	0.0097(8	0.0103(9)	0.012(2)	0.010(1)
				O1			
x	0.1130(3)	0.108(4)	0.105(3)	0.110(3)	0.112(4)	0.109(8)	0.108(8)
y	0.0882(1)	0.0871(6)	0.0864(6)	0.0862(3)	0.0856(6)	0.087(1)	0.087(1)
z	0.1625(5)	0.165(3)	0.165(3)	0.161(3)	0.155(3)	0.162(7)	0.162(6)
U_{iso}/U_{eq}	0.0089(5)	0.009(2)	0.012(2)	0.011(1)	0.014(2)	0.015(4)	0.021(4)
				O2			
x	0.1242(3)	0.122(4)	0.124(3)	0.129(3)	0.131(3)	0.122(8)	0.115(8)
y	0.1743(1)	0.1733(7)	0.1724(7)	0.1714(6)	0.1700(7)	0.173(1)	0.171(1)
z	0.6660(5)	0.668(3)	0.669(3)	0.666(3)	0.664(3)	0.660(6)	0.666(6)
U_{iso}/U_{eq}	0.0097(5)	0.009(2)	0.012(2)	0.011(1)	0.014(2)	0.015(4)	0.021(4)
				O3			
x	0.1145(4)	0.106(5)	0.111(4)	0.116(4)	0.112(4)	0.131(9)	0.127(9)
y	0	0	0	0	0	0	0
z	0.6619(7)	0.662(4)	0.660(4)	0.660(3)	0.655(4)	0.650(8)	0.662(7)
U_{iso}/U_{eq}	0.0110(7)	0.009(2)	0.012(2)	0.011(1)	0.014(2)	0.015(4)	0.021(4)
				O4			
x	0.3812(3)	0.387(3)	0.384(3)	0.380(3)	0.372(3)	0.374(7)	0.381(6)
y	0.2428(1)	0.2436(7)	0.2463(8)	0.2463(7)	0.2482(7)	0.248(1)	0.246(1)
z	0.6851(4)	0.691(2)	0.689(2)	0.685(2)	0.682(2)	0.675(5)	0.679(5)
U_{iso}/U_{eq}	0.0121(5)	0.009(2)	0.012(2)	0.011(1)	0.014(2)	0.015(4)	0.021(4)
				O5			
x	0.3452(3	0.350(3)	0.353(3)	0.350(3)	0.348(3)	0.353(7)	0.363(7)
y	0.1236(2)	0.1240(7)	0.1256(7)	0.1266(6)	0.1259(7)	0.127(1)	0.126(1)
z	0.4117(5)	0.412(2)	0.401(3)	0.399(2)	0.400(2)	0.399(5)	0.402(4)
U_{iso}/U_{eq}	0.0135(6)	0.009(2)	0.012(2)	0.011(1)	0.014(2)	0.015(4)	0.021(4)
				O6			
x	0.3474(3)	0.345(3)	0.347(3)	0.352(3)	0.353(3)	0.361(7)	0.357(7)
y	0.1238(2)	0.1241(7)	0.1237(7)	0.1231(6)	0.1233(7)	0.121(1)	0.119(1)
z	0.9161(5)	0.916(2)	0.905(3)	0.907(2)	0.901(2)	0.898(5)	0.898(4)
U_{iso}/U_{eq}	0.0146(6)	0.009(2)	0.012(2)	0.011(1)	0.014(2)	0.015(4)	0.021(4)
				O7			
x	0.3377(4)	0.333(4)	0.339(4)	0.345(4)	0.344(4)	0.344(9)	0.356(9)
y	0	0	0	0	0	0	0
z	0.1630(7)	0.165(4)	0.168(4)	0.166(3)	0.164(3)	0.170(8)	0.170(7)
U_{iso}/U_{eq}	0.0127(7)	0.009(2)	0.012(2)	0.011(1)	0.014(2)	0.015(4)	0.021(4)
				H			
x	0.031(5)						
y	0						
z	0.75(1)						
U_{iso}/U_{eq}	0.05						

Note: The e.s.d. values in parentheses refer to the last digit.
* Sample in DAC.
† The occupancies of M sites were as follows: M1 83% Fe + 17% Mg; M2 73% Fe + 27% Mg; M3 80% Fe + 20% Mg; M4 72% Mn + 28% Fe.

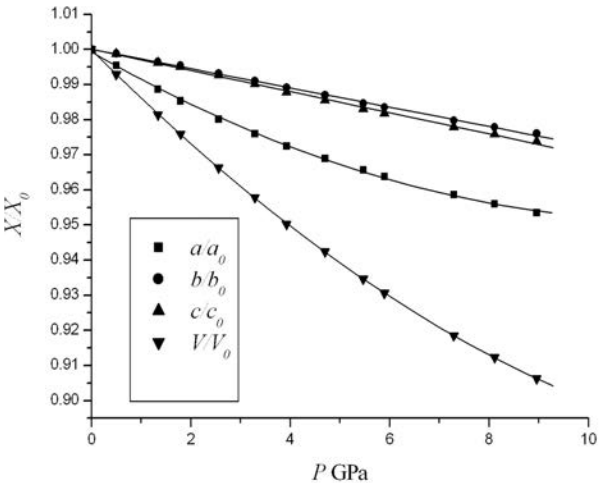

FIGURE 2. Unit-cell parameters of protomangano-ferro-anthophyllite as a function of pressure. Data normalized with respect to room-pressure values. Estimated standard deviations are smaller than symbols.

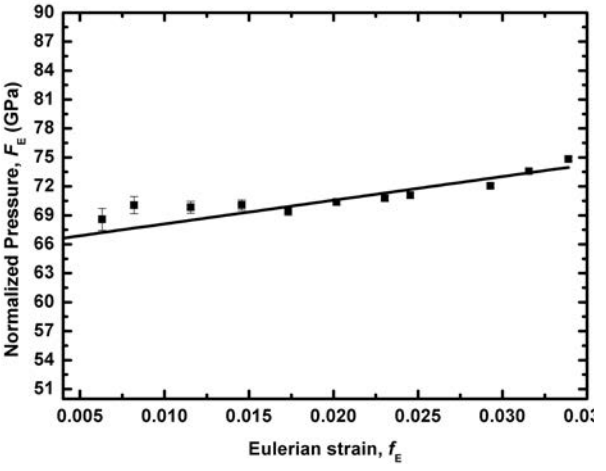

FIGURE 3. Plot of normalized stress, defined as $F_E = P/[3f_E(1 + 2f_E)^{5/2}]$ vs. finite strain $f_E = [(V_0/V)^{2/3} - 1]/2$.

of the *a* parameter (Fig. 4).

The M polyhedra show similar compressibility, owing to their similar composition. M4, which presents a large distortion, is slightly softer than the other octahedra (M1, M2, M3). Crystal-chemical studies of amphiboles (Hawthorne and Oberti 2007) have shown that the M4 site is significantly affected by the requirements of dimensional matching between the octahedral strip and the tetrahedral double-chain. In *Pnmn* amphibole, as in grunerite, the M4 cation is actually in a distorted fourfold coordination with no connectivity to the double tetrahedral chains (Sueno et al. 1998), as results from calculation of procrystal electron density distribution and the critical bond-path analysis (Bader 1990). From a geometrical point of view, the M4 site is surrounded by six oxygen atoms, in a 4+2 configuration (Table 6). As pressure increases, the longest M4-O6 distances decrease significantly, and the coordination of M4 site tends effectively to become sixfold. M1, M2, and M3 octahedra have similar

TABLE 6. Relevant bond lengths (Å), polyhedral volumes, and distortion coefficients (following Robinson et al. 1971) of protomangano-ferro-anthophyllite at various pressures

P (GPa)	0.0001	0.0001*	1.54	2.23	3.92	6.02	6.93
T1-O1	1.618(3)	1.66(4)	1.71(3)	1.67(3)	1.64(3)	1.62(6)	1.62(6)
T1-O5	1.618(3)	1.63(2)	1.61(2)	1.60(2)	1.58(2)	1.65(4)	1.66(4)
T1-O6	1.629(3)	1.65(2)	1.63(2)	1.63(2)	1.63(2)	1.62(4)	1.61(4)
T1-O7	1.618(2)	1.61(1)	1.60(1)	1.61(1)	1.60(1)	1.60(3)	1.64(3)
<T1-O>	1.621	1.62	1.64	1.63	1.61	1.62	1.63
V (Å^3)	2.183(8)	2.19(5)	2.26(5)	2.20(5)	2.16(5)	2.17(8)	2.21(8)
λ†	1.000	1.000	1.001	1.001	1.000	1.003	1.006
σ^2‡	1.08	1.0	0.9	0.8	0.5	11.5	26.1
T2-O2	1.623(3)	1.64(3)	1.62(3)	1.59(3)	1.55(3)	1.61(6)	1.62(6)
T2-O4	1.603(3)	1.65(2)	1.66(2)	1.62(2)	1.61(2)	1.60(4)	1.61(4)
T2-O5	1.628(3)	1.64(2)	1.63(2)	1.62(2)	1.59(2)	1.60(4)	1.64(4)
T2-O6	1.657(3)	1.65(2)	1.62(2)	1.64(2)	1.62(2)	1.65(4)	1.66(3)
<T2-O>	1.628	1.63	1.63	1.62	1.59	1.60	1.63
V (Å^3)	2.196(8)	2.20(5)	2.21(5)	2.15(5)	2.07(5)	2.09(8)	2.21(8)
λ†	1.005	1.005	1.006	1.005	1.004	1.002	1.008
σ^2‡	20.59	21.1	23.0	17.8	14.7	8.52	35.8
M1-O1(×2)	2.096(2)	2.06(2)	2.03(2)	2.07(2)	2.09(2)	2.04(5)	2.02(5)
M1-O2 (×2)	2.161(2)	2.14(2)	2.14(2)	2.14(2)	2.13(2)	2.10(4)	2.06(4)
M1-O3 (×2)	2.126(2)	2.09(2)	2.08(2)	2.10(2)	2.04(2)	2.10(5)	2.09(5)
<M1-O>	2.128	2.10	2.09	2.10	2.09	2.08	2.06
V (Å^3)	12.65(1)	12.1(1)	11.8(1)	12.2(1)	11.9(1)	11.9(2)	11.4(2)
λ†	1.010	1.017	1.018	1.009	1.010	1.007	1.012
σ^2‡	34.42	53.4	54.4	32.0	34.0	23.1	39.5
M2-O1 (×2)	2.170(2)	2.17(2)	2.13(2)	2.14(2)	2.12(2)	2.09(4)	2.08(4)
M2-O2 (×2)	2.139(2)	2.12(2)	2.11(2)	2.14(2)	2.15(2)	2.10(5)	2.04(5)
M2-O4 (×2)	2.065(2)	2.04(2)	2.02(2)	2.03(2)	2.04(2)	1.98(4)	1.99(4)
<M2-O>	2.124	2.11	2.09	2.10	2.10	2.08	2.04
V (Å^3)	12.58(1)	12.3(1)	11.8(1)	12.2(1)	12.2(1)	11.7(2)	11.0(2)
λ†	1.011	1.017	1.018	1.013	1.011	1.012	1.017
σ^2‡	36.74	55.9	57.9	40.7	35.5	40.0	56.6
M3-O1(×4)	2.124(2)	2.09(2)	2.06(2)	2.06(2)	2.03(1)	2.04(4)	2.03(4)
M3-O3 (×2)	2.106(4)	2.07(3)	2.08(3)	2.10(2)	2.09(3)	2.20(7)	2.11(6)
<M3-O>	2.118	2.09	2.07	2.07	2.05	2.09	2.06
V (Å^3)	12.37	11.7(1)	11.3(1)	11.5(1)	11.2(1)	11.9	11.3
λ†	1.016	1.024	1.029	1.018	1.018	1.019	1.018
σ^2‡	52.95	75.6	89.9	59.2	57.8	53.5	58.6
M4-O2 (×2)	2.160(2)	2.17(2)	2.18(2)	2.20(2)	2.21(2)	2.11(4)	2.11(4)
M4-O4 (×2)	2.024(2)	1.97(2)	1.98(2)	2.01(2)	2.06(2)	2.07(4)	2.00(4)
M4-O6 (×2)	2.603(3)	2.62(2)	2.60(2)	2.58(2)	2.56(2)	2.53(4)	2.57(4)
<M4-O>	2.262	2.25	2.26	2.27	2.28	2.24	2.23
V (Å^3)	12.08(1)	11.9(1)	11.7(1)	11.8(1)	11.7(1)	11.0(2)	10.8(2)
λ†	1.192	1.193	1.214	1.209	1.225	1.239	1.246
σ^2‡	383.81	384.2	422.7	413.1	442.1	457.9	477.4
V A site (Å^3)	41.05(2)	41.7(1)	39.4(1)	38.7(1)	37.5(1)	35.3(3)	33.4(3)
O4-O4′§	2.244(4)	2.18(2)	2.17(2)	2.23(2)	2.24(2)	2.30(4)	2.16(4)
O7-O7′§	3.065(4)	3.16(2)	2.98(2)	2.87(2)	2.87(2)	2.83(4)	2.61(4)
O5-O6-O5′(°)	179.1(2)	178(2)	177(1)	177(1)	177(1)	174(3)	174(2)
T1-O7-T1 (°)	143.8(3)	146(3)	145(2)	142(3)	144(3)	141(6)	134(5)
α (°)‖	0.2(2)	0.2(8)	2.0(8)	2.9(8)	2.9(8)	4(2)	4(2)

* Sample in DAC.
† λ is the quadratic elongation.
‡ σ^2 is the angle variance (°^{2}).
§ These distances are the components of O4-O4′ and O7-O7′ distances along the [100] direction.
‖ α is the tetrahedral rotation angle; see text for definition.

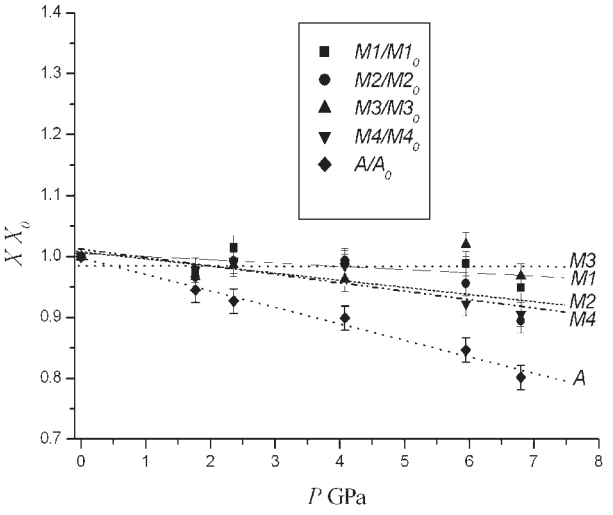

FIGURE 4. Polyhedral volumes in protomangano-ferro-anthophyllite (normalized to room-*P* value) according to pressure.

compressibilities, M2 being slightly softer (Fig. 4), which may arise from the Fe content of the site, which is about 73%, compared with 83 and 80% at M1 and M3, respectively. The relative compressibilities of M octahedra for other amphiboles reported in the literature are M3 > M1 > M2 in glaucophane, M2 > M1 > M3 in tremolite and pargasite (Comodi et al. 1991), and M2 > M3 > M1 and M2 > M1 > M3 in two kaersutites with a different oxo-component (Comodi et al. 2010). These trends show that the compressibilities of the various components of the cation ribbon depends significantly on composition.

The tetrahedra do not undergo significant changes in the pressure range studied here, as expected on the basis of the Si-O bond strength. The major changes involving tetrahedra concern kinking of the double chain, bending along the [100] direction through the empty A site, and tetrahedral rotation, all necessary to maintain coherence with the octahedral ribbon. In protoamphibole, the tetrahedral chain is fully extended along the **c** direction. A measure of kinking is the angle O5-O6-O5, which in air is 179.1(2)°, very near the value of 180° of a completely extended chain. This angle decreases to 174(2)° at 6.9 GPa. The double chain loses its slight concavity around the A site, becoming flatter, which is registered by the shortening of the projection of the O7-O7′ distance in the [100] direction, compared with the decrease in the component of the O4-O4′ distance along **a** (Table 6; Fig. 1). The O7-O7′ distance decreases by 15%, from 3.065(2) Å at 1 atm to 2.61(1) Å at 6.9 GPa, whereas the O4-O4′ distance decreases by 4%, from 2.244(2) to 2.16(1) Å. The difference Δ = (O7-O7′) – (O4-O4′) decreases from 0.82 to 0.46 Å, with a consequent decrease in the bowing of the tetrahedral chains at 6.9 GPa.

The same mechanism is shown by the evolution of the T1-O7-T1 angle [from 143.8(3)° to 134(5)° at 6.9 GPa]. Increasing *P* also affects tetrahedral rotation α, defined as half the difference between the average of the three larger and the three smaller O-O-O angles in the pseudo-hexagon of the double tetrahedral chain: α increases from 0.2(2)° to 4(2)° (Table 7). Tetrahedral rotation explains the reduction in the M4-O6 distance, from 2.606(3) to 2.57(4) Å at 6.8 GPa.

Our results can be compared with those reported in the literature for other amphiboles (Table 7). As most of these studies used a second-order Birch-Murnaghan equation-of-state (*K*' fixed at 4), to allow a meaningful comparison the bulk modulus of protoamphibole was recalculated with a second-order Birch-

TABLE 7. Bulk moduli (K_{T0}) and their pressure-derivative $K\alpha$ of some amphiboles

Amphibole	Space group	K_{T0} GPa	K'	Reference
Protoamphibole	*Pnmn*	64(1)	7.0(4)	present work
Protoamphibole	*Pnmn*	74(1)	4	present work
Cummingtonite	$P2_1/m$	62.4(5)	8.2(2)	Boffa Ballaran et al. (2000)
Cummingtonite	*C2/m*	66(2)	8.2	Boffa Ballaran et al. (2000)
Cummingtonite	$P2_1/m$	71(1)	6.1(5)	Yang et al. (1998)
Cummingtonite	*C2/m*	78(3)	4	Yang et al. (1998)
Grunerite	*C2/m*	63(1)	4	Zhang et al. (1992)
Grunerite	*C2/m*	50(1)	13(1)	Zhang et al. (1992)
Grunerite-cummingtonite *s.s.*	*C2/m*-$P2_1/m$	65.4(1.9)	7.0(4)	Boffa Ballaran et al. (2000)
Tremolite	*C2/m*	76(3)	4	Comodi et al. (1991)
Pargasite	*C2/m*	89(3)	4	Comodi et al. (1991)
Glaucophane	*C2/m*	88(6)	4	Comodi et al. (1991)
K-richterite	*C2/m*	89(3)	4	Welch et al. (2007)
Kaersutite FR12 (oxo)	*C2/m*	94(1)	6.3(4)	Comodi et al. (2010)
Kaersutite FR12 (oxo)	*C2/m*	100.5(8)	4	Comodi et al. (2010)
Kaersutite DL5	*C2/m*	91(2)	6.2(4)	Comodi et al. (2010)
Kaersutite DL5	*C2/m*	96.8(7)	4	Comodi et al. (2010)

Murnaghan EoS, which gives the following parameters: V_0 = 924.5(7) Å^3, K_{T0} = 74(1) GPa. This bulk modulus is very similar to those found for cummingtonite polymorphs (Yang et al. 1998). As Table 7 shows, the HP behavior of amphiboles is mainly a function of the compressibility of the A site and the different response of the bending deformation of the double chain of tetrahedra. Amphiboles with empty A sites (tremolite, cummingtonite, grunerite, and protoamphibole) are much more compressible than ones with filled A sites, such as pargasite, K-richterite, and kaersutite.

ACKNOWLEDGMENTS

The constructive reviews by the Associate Editor (M.D. Dyar) and the journal referees (M. Welch and an anonymous referee) greatly contributed to improve the manuscript. The English text was revised by Gabriel Walton.

REFERENCES CITED

Angel, R.J. (2000) Equation of State. In R.M. Hazen and R.T. Downs, Eds., High-Temperature and High-Pressure Crystal Chemistry, 41, p. 35–59. Reviews in Mineralogy and Geochemistry, Mineralogical Society of America and Geochemical Society, Chantilly, Virginia.

——— (2004a) Program for absorption. Crystallography Laboratory, Department Geological Sciences, Virginia Tech, Blacksburg, Virginia, U.S.A.

——— (2004b) EOS-FIT V6.1. Computer program. Crystallography Laboratory, Department Geological Sciences, Virginia Tech, Blacksburg, U.S.A.

Angel, R.J., Allan, D.R., Miletich, R., and Finger, L.W. (1997) The use of quartz as an internal pressure standard in high pressure crystallography. Journal of Applied Crystallography, 30, 461–466.

Bader, R.F.W. (1990) Atoms in molecules. Oxford Science Publications, Oxford, U.K.

Boffa Ballaran, T., Angel, R.J., and Carpenter, M.A. (2000) High-pressure transformation behaviour of the cummingtonite-grunerite solid solution. European Journal of Mineralogy, 12, 1195–1213.

Budzianowski, A. and Katrusiak, A. (2004) High-pressure crystallographic experiments with a CCD-detector. In A. Katrusiak and P. McMillan, Eds., High-Pressure Crystallography, p. 101–112. Kluwer, Dordrecht.

Comodi, P., Mellini, M., Ungaretti, L., and Zanazzi, P.F. (1991) Compressibility and high pressure structure refinement of tremolite, pargasite, and glaucophane. European Journal of Mineralogy, 3, 485–499.

Comodi, P., Boffa Ballaran, T., Zanazzi, P.F., Capalbo, C., Zanetti, A., and Nazzareni, S. (2010) The effect of oxo-component on the high-pressure behavior of amphiboles. American Mineralogist, 95, 1042–1051.

Gibbs, G.V. (1969) The crystal structure of protoamphibole. Mineralogical Society of America, Special Paper, 2, 101–109.

Gibbs, G.V., Bloss, F.D., and Shell, H.R. (1960) Proto-amphibole, a new polytype. American Mineralogist, 45, 974–988.

Hawthorne, F.C. (1981) Crystal chemistry of the amphiboles. In D.R. Veblen, Ed., Amphiboles and Other Hydrous Pyriboles Mineralogy, 9A, p. 1–102. Reviews in Mineralogy, Mineralogical Society of America, Chantilly, Virginia.

Hawthorne, F.C. and Oberti, R. (2007) Amphiboles: Crystal chemistry. In F.C. Hawthorne, R. Oberti, G. Della Ventura, and A. Mottana, Eds., Amphiboles: Crystal chemistry, occurrence, and health issues, 67, p. 1–54. Reviews in Mineralogy and Geochemistry, Mineralogical Society of America and Geochemical Society, Chantilly, Virginia.

Hawthorne, F.C., Oberti, R., Della Ventura, G., and Mottana, A., Eds. (2007) Amphiboles: Crystal chemistry, occurrence and health issues, 67, 545 p. Reviews in Mineralogy and Geochemistry, Mineralogical Society of America and Geochemical Society, Chantilly, Virginia.

Ionov, D.A., Bodinier, J.-L., Mukasa, S.B., and Zanetti, A. (2002) Mechanisms and sources of mantle metasomatism: Major and trace element compositions of peridotite xenoliths from Spitsbergen in the context of numerical modeling. Journal of Petrology, 43, 2219–2259.

Ionov, D.A. and Hofmann, A.W. (1995) Nb-Ta-rich mantle amphiboles and micas: Implications for subduction-related metasomatic trace element fractionations. Earth and Planetary Science Letters, 131, 341–356

Jeanloz, R. and Hazen, R.M. (1991) Finite-strain analysis of relative compressibilities. Application to the high-pressure wadsleyite phase as an illustration. American Mineralogist, 76, 1765–1768.

King, H.E. and Finger, L.W. (1979) Diffracted beam crystal centering and its application to high-pressure crystallography. Journal of Applied Crystallography, 12, 374–378.

Matsuura, S. and Sueno, S. (1984) The crystal structure of iron amphibole with the space group Pnmn. Mineralogical Society of Japan, 1984 Annual Meeting Abstract, p. 128 (in Japanese).

Matsuura, S., Sueno, S., and Bunno, M. (1985) The crystal chemistry of Fe-Mn amphiboles with proto-type structure. Mineralogical Society of Japan, 1985 Annual Meeting Abstract, p. 63 (in Japanese).

Miletich, R., Reifler, H., and Kunz, M. (1999) The "ETH diamond-anvil cell" design for single-crystal XRD at non-ambient conditions. Acta Crystallographica, A55, 99–100.

Niida, K. and Green, D.H. (1999) Stability and chemical composition of pargasitic amphibole in MORB pyrolite under upper mantle conditions. Contributions to Mineralogy and Petrology, 135, 18–40.

Pouchou, J.L. and Pichoir, F. (1985) PAP phi-rho-Z procedure for improved quantitative microanalysis. In J.L. Armstrong, Ed., Microbeam Analysis, p. 104–106. San Francisco Press Inc., California.

Robinson, K., Gibbs, G.V., and Ribbe, P.H. (1971) Quadratic elongation, a quantitative measure of distortion in coordination polyhedra. Science, 172, 191–193.

Sheldrick, G.M. (1996) SADABS. Program for empirical absorption correction of area detector data. Institut für Anorganische Chemie, University of Göttingen, Germany.

——— (1997) SHELX-97. Programs for crystal structure determination and refinement. Institut für Anorganische Chemie, University of Göttingen, Germany.

Sueno, S., Matsuura, S., Gibbs, G.V., and Boisen, Jr., M.B. (1998) A crystal chemical study of protoanthophyllite: Orthoamphibole with the protoamphibole structure. Physics and Chemistry of Minerals, 25, 366–377.

Sueno, S., Matsuura, S., Bunno, M., and Kurosawa, M. (2002) Occurrence and crystal chemical features of protoferro-anthophyllite and protomanganoferro-anthophyllite from Cheyenne Canyon and Cheyenne Mountain, U.S.A. and Hirukawa-mura, Suisho-yama, and Yokone-yama, Japan. Journal of Mineralogical and Petrological Sciences, 97, 127–136.

Thompson, Jr., J.B. (1970) Geometrical possibilities for amphibole structures: Model biopyriboles. American Mineralogist, 55, 292–293.

Vannucci, R., Piccardo, G.B., Rivalenti, G., Zanetti, A., Rampone, E., Ottolini, L., Oberti, R., Mazzucchelli, M., and Bottazzi, P. (1995) Origin of LREE-depleted

amphiboles in the subcontinental mantle. Geochimica and Cosmochimica Acta, 59, 1763–1771.
Wallace, M.E. and Green, D.H. (1991) The effect of bulk rock composition on the stability of amphibole in the upper mantle: Implication for solidus positions and mantle metasomatism. Mineralogy and Petrology, 44, 1–19.
Welch, M.D., Cámara, F., Della Ventura, G., and Iezzi, G. (2007) Non-ambient in situ studies of amphiboles. In F.C. Hawthorne, R. Oberti, G. Della Ventura, and A. Mottana, Eds., Amphiboles: Crystal chemistry, occurrence and health issues, 67, p. 223–260. Reviews in Mineralogy and Geochemistry, Mineralogical Society of America and Geochemical Society, Chantilly, Virginia.
Wilson, A.J.C. and Prince, E. (1999) International Tables for X-ray Crystallography, Volume C: Mathematical, physical and chemical tables (2nd edition). Kluwer, Dordrecht.
Yang, H., Hazen, R.M., Prewitt, C.T., Finger, L.W., Lu, R., and Hemley, R.J. (1998) High-pressure single-crystal X-ray diffraction and infrared spectroscopic studies of the $C2/m$-$P2_1/m$ phase transition in cummingtonite. American Mineralogist, 83, 288–299.
Zhang, L., Ahsbahs, H., Kutoglu, A., and Hafner, S.S. (1992) Compressibility of grunerite. American Mineralogist, 77, 480–483.

Manuscript received March 23, 2010
Manuscript accepted June 20, 2010
Manuscript handled by M. Darby Dyar